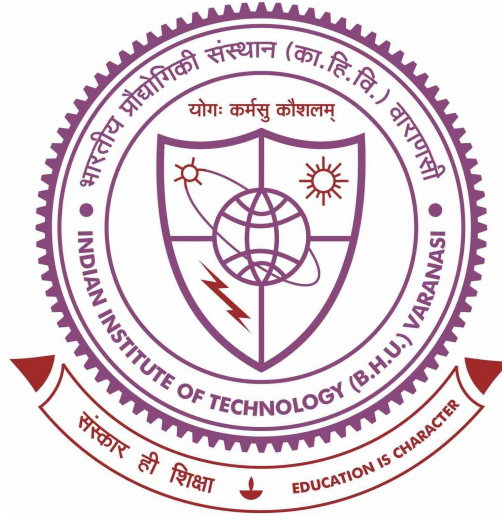


# **Understanding the variabilities of the magnetic cycles of solar-type stars through dynamo modelling**



**Thesis submitted in partial fulfilment**

**for the Award of**

**DOCTOR OF PHILOSOPHY**

**in**

**PHYSICS**

**by**

**VINDYA VASHISHTH**

**DEPARTMENT OF PHYSICS**

**INDIAN INSTITUTE OF TECHNOLOGY**

**(BANARAS HINDU UNIVERSITY)**

**VARANASI – 221 005**

**ROLL NUMBER**  
19171018

**YEAR OF SUBMISSION**  
2025

## CERTIFICATE

It is certified that the work contained in the thesis titled **Understanding the variabilities of the magnetic cycles of solar-type stars through dynamo modelling** by **Vindya Vashishth** has been carried out under my supervision and that this work has not been submitted elsewhere for a degree.

It is further certified that the student has fulfilled all the requirements of the Comprehensive Examination, Candidacy, and SOTA for the award of **Doctor of Philosophy**.

*Bidyabinay Karak*

**Supervisor**

**Dr. Bidya Binay Karak**

Department of Physics

Indian Institute Of Technology

(Banaras Hindu University)

Varanasi - 221 005

**Associate Professor**

Department of Physics

Indian Institute of Technology

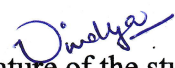
(Banaras Hindu University)

Varanasi-221005

## DECLARATION BY THE CANDIDATE

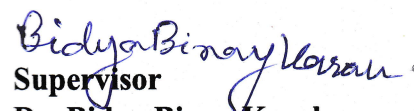
I, **Vindya Vashishth**, certify that the work embodied in this thesis is my own bonafide work and carried out by me under the supervision of **Dr. Bidya Binay Karak** from 2019 to 2025, at the **Department of Physics**, Indian Institute of Technology (Banaras Hindu University), Varanasi. The matter embodied in this thesis has not been submitted for the award of any other degree/diploma. I declare that I have faithfully acknowledged and given credits to the research workers wherever their works have been cited in my work in this thesis. I further declare that I have not willfully copied any other's work, paragraphs, text, data, results, *etc.*, reported in journals, books, magazines, reports, dissertations, theses, *etc.*, or available at websites and have not included them in this thesis and have not cited as my own work.

Date: 16/07/2025  
Place: IIT (BHU) Varanasi, India

  
Signature of the student  
(Vindya Vashishth)

## CERTIFICATE BY THE SUPERVISOR

It is certified that the above statement made by the student is correct to the best of my knowledge.

  
**Supervisor**  
**Dr. Bidya Binay Karak**  
Department of Physics  
Indian Institute Of Technology  
(Banaras Hindu University)  
Varanasi – 221 005  
**Associate Professor**  
Department of Physics  
Indian Institute of Technology  
(Banaras Hindu University)  
Varanasi-221005

  
**Signature of Head of Department (Physics)**

HEAD/विभागाध्यक्ष  
भौतिकी विभाग/Deptt. of Physics  
आ०प्रौ०सं०/(का०हि०वि०)/IIT-(BHU)  
वाराणसी/Varanasi-221005

## COPYRIGHT TRANSFER CERTIFICATE

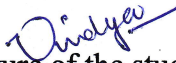
**Title of the Thesis:** Understanding the variabilities of the magnetic cycles of solar-type stars through dynamo modelling

**Name of the Student:** Vindya Vashishth

## COPYRIGHT TRANSFER

The undersigned hereby assigns to the Indian Institute of Technology (Banaras Hindu University), Varanasi all rights under copyright that may exist in and for the above thesis submitted for the award of the Doctor of Philosophy in Physics.

Date: 16/07/2025  
Place: IIT (BHU) Varanasi, India

  
Signature of the student  
(Vindya Vashishth)

**Note:** However, the author may reproduce or authorize others to reproduce material extracted verbatim from the thesis or derivative of the thesis for author's personal use provided that the source and the Institute's copyright notice are indicated.

*I dedicate this thesis to  
my beloved family*

## ACKNOWLEDGEMENTS

---

प्रथमवयसि दत्तं तोयमल्पं स्मरन्तः शिरसि निहितभारा नारिकेला नराणाम् ।

सलिलममृतकल्पं दद्युराजीवनान्तं न हि कृतमुपकारं साधवो विस्मरन्ति ॥

**Meaning:** *Remembering the water given in their early growth, coconut trees bear burdens and provide sweet water throughout life. Similarly, a virtuous person never forgets even the smallest kindness and help.*

---

Inspired by this sentiment, I express my heartfelt gratitude to everyone who has ever contributed to my academic journey and the completion of this thesis.

First, I sincerely thank my Guru and thesis supervisor, **Dr. Bidya Binay Karak**, for his invaluable guidance, insightful discussions, and unwavering support throughout my doctoral journey. His encouragement and expertise have been instrumental in shaping my research and academic growth. His ability to balance meticulous attention to detail with a broader scientific perspective has set an example I aspire to follow in my future endeavors. I am also deeply grateful for his support in helping me identify and pursue the right opportunities, such as conferences and workshops, which have significantly broadened my knowledge and expanded my professional network. I now thank the **Almighty God** for their blessings and support, not only in my academic journey but throughout my life.

Moving ahead, I express my gratitude to the **Head of the Department (Prof. Sandeep Chatterjee)** and Research Progress Evaluation Committee (RPEC) members (**Dr. Abhishek Kumar Shrivastava** and **Dr. Somak Bhattacharaya**), and all faculty members of the Department of Physics, Indian Institute of Technology (BHU), Varanasi, for providing a conducive research environment and the necessary resources for my work. I also want to

---

thank the administrative staff, library personnel, and the Param Shivay computational support team for their invaluable assistance and facilities they have provided for my research endeavors.

I extend my heartfelt thanks to my collaborator, **Prof. Leonid L. Kitchatinov** for providing the data from his model, carefully reviewing the manuscripts, offering valuable and constructive feedback, and raising insightful questions that have significantly enhanced the quality of my thesis work.

Special thanks to my labmates, **Anu B Sreedevi, Dr. Pawan Kumar, Akash Biswas, Rambahadur Gupta, and Rohan B Mandrai** for their valuable input, unconditional support, insightful discussions, and assistance throughout my doctoral journey. I feel fortunate to have worked alongside such a talented and supportive group of individuals. The memories of our fun moments, celebrations, and explorations of new places will remain unforgettable.

This journey would have been incomplete without the unwavering support of my dear friends. I am deeply thankful to my roommate, **Smrati Pandey**, for her love and support over the past two years. She has been like the sister I never had, offering unbiased opinions and standing by me through every high and low. I will always cherish our adventures through the streets of Varanasi, indulging in delightful foods together. I wish her all the best for her remaining doctoral journey. I extend my gratitude to **Samikhsha, Manisha, Kartika, Nidhi, Sarita, Neelam, Pawan, Ashish, Sachin, and Pammi**, for their constant presence and support throughout my doctoral journey. Meeting them in Varanasi was a turning point, and they have become an integral part of my life and academic experience. Some people provide immense life support even in their physical absence. I want to express my love and gratitude to my school and college friends: **Shruti, Abhaya, Neelam, Lakshita, Shagun, Monika, Shiwani and Anupam**. Their friendship has been a constant source of motivation and solace, making this journey more meaningful and memorable.

I also thank **Dr. Kirti Batra**, for her constant guidance throughout my academic journey. This journey would also have been incomplete without the love and support of my hus-

---

band, **Arun Sharma**, and his parents. Arun has been my steady support, trusted friend, and constant critic. His encouragement and thoughtful insights have enriched my journey, and I am deeply grateful for his belief in me and my work.

Finally, I would like to thank the three most important people in my life: my parents (**Neeru and Mukesh Vashishth**) and younger brother **Ashutosh** (my Ashu). I dedicate this thesis to them, whose patience, unwavering encouragement, and the values they instilled in me have been the foundation of my journey. Their sacrifices, encouragement, patience, and belief in my abilities have been my guiding light. Their unconditional love and support allowed me to complete this challenging journey. Their boundless love and support have served me with positive energy on this doctoral journey.

# List of Figures

1.1	HR Diagram reproduced using HIPPARCOS catalog. . . . .	2
1.2	Activity-rotation relation in solar-like stars in terms of fractional X-ray luminosity ( $R_X$ ) vs. (a) the rotation period, and (b) the Rossby number ( $R_o$ ) of solar-type stars. Image credit: Wright et al. (2011). . . . .	5
1.3	Full-disk images of sunspots on the solar surface. The left image is a colorized magnetogram of the Sun (at 6173 Å spectral line of Fe I with a color table ranging from -1500 G to 1500 G. Fields weaker than 24 G are shown in grey, while green and blue represent positive fields, and yellow and red indicate negative fields), highlighting the magnetic activity of the sunspots visible in the white-light image (intensity continuum) on the right. Image credit: NASA: SDO/HMI. . . . .	8
1.4	Spherical projection of the average temperature map of the K0 III star, XX Trianguli (HD 12545), illustrating the starspots. The size of the solar disk is included on the upper left for comparison. On the right, small panels present temperature profiles along both longitudinal and latitudinal cuts through the warm and cool spots. Image Credit: Strassmeier et al. (1999)	9
1.5	Starspots identified using the interferometric map of a K-giant $\sigma$ Gemino- rum from 2011 (left) and 2012 (right), Image credit: Roettenbacher et al. (2017) . . . . .	10
1.6	Solar cycle: Variation of the number of sunspot (red dotted curve)/sunspot areas/sunspot group number(black curve). Image credit: Karak (2023a). .	11

1.7	Representation of a few good cycles from old to intermediate stars of spectral type G and K as measured by the MWO-calibrated Ca II emission fluxes (S-index). Red and blue curves are the fitted profiles given in Garg et al. (2019) . . . . .	11
1.8	A few examples of stellar cycles of old stars depicting flat-like activity as identified by Baliunas et al. (1995). Vertical axis shows the Ca II emission in S-index unit. . . . .	12
1.9	Same as Fig. 1.8 but for some stars which show irregular cycles as identified by Baliunas et al. (1995). . . . .	12
1.10	Magnetic butterfly diagram: Longitudinally averaged distribution of the surface radial field over the past four solar cycles, obtained from instruments on Kitt Peak, SOHO and SDO. Image credit: Dr. David H. Hathaway via <a href="http://www.solarcyclescience.com">www.solarcyclescience.com</a> . . . . .	14
1.11	Cycle period vs rotation period: Red, green, and black symbols represent stars with well-defined cycles, multiple or chaotic cycles, and unconfirmed cycles, respectively, based on data from Mount Wilson (solid circles) and HARPS (solid triangles). Vertical green lines connect the two cycle periods of a star exhibiting dual cycles. The dotted lines depict the active and inactive branches of stellar activity cycles, as described by Böhm-Vitense (2007). Sun is marked as $\odot$ . Image credit: Boro Saikia et al. (2018). . . . .	16
1.12	S-index time series for K2V star, HD 166620 showing entering into Maunder minimum phase. Blue points depict data from Mount Wilson, and green points show from the Keck HIRES. Image Credit: Baum et al. (2022) . . . . .	17
1.13	Solar differential rotation (left) and rotation profiles at constant latitudes as a function of radius (right), obtained from the global helioseismic analyses. Image credit: GONG data, Howe (2009). . . . .	19

1.14	Solar meridinal circulation streamlines (left) and its variation with depth at $45^\circ$ latitude (right). This image is obtained from hydrodynamic mean-field model of Kitchatinov & Olemskoy (2011b). . . . .	22
1.15	Pictorial illustration of cyclic variation of stellar magnetic field as per observations. . . . .	23
1.16	Pictorial illustration of the $\Omega$ effect . . . . .	27
1.17	Pictorial illustration of the $\alpha$ effect: (I) (a) $\Omega$ effect (refer Fig. 1.16 for generation of the toroidal field) (b) Rising and twisting of field lines (refer to II for a clearer view) (c) Generation of the poloidal field through the merging the eddies (Inspired by (Choudhuri, 1998)). . . . .	29
1.18	Pictorial illustration of the Babcock–Leighton process: The BMR deposit of the surface (leftmost image) decays and is dispersed (middle image) and forms the poloidal field of the opposite polarity (rightmost). Image credit: (Charbonneau & Sokoloff, 2023). . . . .	34
1.19	Pictorial representation of the solar/stellar dynamo theory. Image credit: Noraz et al. (2022a) . . . . .	35
1.20	Cyclic representataion of the solar/stellar dynamo theory . . . . .	36
2.1	Dynamo hysteresis: Variation of the temporal average of the mean toroidal field normalized to $B_0$ and computed at the BCZ at latitude $-14^\circ$ ( $B_{avg}$ ) as a function of $\alpha_0$ (in $\text{m s}^{-1}$ ) from simulations started with a weak field (filled circles) and from simulations started with strong field of previous simulation (orange diamonds). The corresponding $D$ is shown in top horizontal axis. . . . .	45
2.2	(a) Time-latitude distribution of the toroidal field at BCZ from a dynamo simulation at critical dynamo case ( $\alpha = 28.10 \text{ m s}^{-1}$ ) for which the simulation started with a weak field. (b) Same as (a) but from a subcritical dynamo case ( $\alpha = 23 \text{ m s}^{-1}$ ) and the simulation started with a strong field. . . . .	47
2.3	Same as Fig. 2.1 but obtained from simulations in which $\alpha_{BL}$ and $\eta_T$ are related to the toroidal field at the BCZ. . . . .	48

2.4 Butterfly diagrams for (a) toroidal field at BCZ for critical dynamo for the case ( $\alpha_0 = 36.40 \text{ m s}^{-1}$ ) when the simulation started with a weak magnetic field and (b) for subcritical dynamo case ( $\alpha_0 = 35 \text{ m s}^{-1}$ ) and started with the output of a strong oscillatory solution at  $\alpha_0 = 36 \text{ m s}^{-1}$ . . . . . 48

2.5 Butterfly diagrams of toroidal field for subcritical dynamo at  $\alpha_0 = 35 \text{ m s}^{-1}$  with 20 percent fluctuations. Note that the duration 80–1130 years, i.e., the time spans shown in between two panels are not displayed. . . . . 50

2.6 (a) Time series plot along with its smoothed curve (yellow) of toroidal magnetic flux. Red horizontal line shows the half of the mean of this smooth curve. (b) & (c) Butterfly diagram of toroidal field for the two grand minima. These are obtained from a supercritical dynamo at  $\alpha_0 = 40 \text{ m s}^{-1}$ . . . . . 51

2.7 Variation of variability with respect to the increase in  $\alpha_0$  with 2% fluctuations (orange solid line) and with 20% fluctuations (blue dashed line). . . . . 52

3.1 (a) Normalized temporal mean of rms value of the large-scale magnetic field and (b) temporal mean of  $u_{\text{rms}}$  as a function of  $\sigma$ . . . . . 60

3.2 Top: Butterfly diagrams of the large-scale magnetic field,  $\overline{B}_y(\pi, z, t)$ . Bottom: Time series plots of  $\overline{B}_y(x, z, t)$  taken from an arbitrarily chosen mesh point as a function of time normalized by the diffusive time  $(k_1^2 \eta)^{-1}$ . These results are from a simulation initiated with a weak seed field at (a)  $\sigma = 0.15$  (Run E, Subcritical) and (b)  $\sigma = 0.16$  (Run F, Critical). . . . . 61

3.3 Top: butterfly diagrams of the small-scale magnetic field,  $\mathbf{b}^2(\pi, z, t)$ . Bottom: time series plots of  $\mathbf{b}^2(x, z, t)$  taken from an arbitrarily chosen mesh point as a function of time normalized by the diffusive time scales. These results are from a simulation initiated with a weak seed field at (a)  $\sigma = 0.15$  (Run E, Subcritical) and (b)  $\sigma = 0.16$  (Run F, Critical). . . . . 62

3.4 Butterfly diagram the large-scale magnetic field,  $\overline{B}_y(\pi, z, t)$  when the simulation started with a strong magnetic field for the subcritical dynamo Run E ( $\sigma = 0.15$ ). . . . . 62

3.5	Time series of the large-scale (black/solid line) and small-scale (red/dash line) fields, when (a) large-scale dynamo is excited, and (b) both large- and small-scale dynamos are excited at the same time. Results of (b) are taken from Run F at $\sigma = 0.16$ (i.e., the critical value in this setup), while in (a), the parameters are the same except the value of $k_f$ and $\nu$ are changed to 5.1 and $10^{-2}$ (Run F'). . . . .	63
3.6	Dynamo hysteresis: Variation of the temporal mean of rms value of the large-scale magnetic field normalized to $B_{eq}$ as a function of helicity parameter $\sigma$ from simulations started with a weak seed field (red filled circles) and from simulations started with a strong field of previous simulation (blue stars). . . . .	64
4.1	Dependence of saturated radial field on meridional circulation amplitude $v_0$ in the 2D dynamo model with explicit $\alpha$ term for Babcock–Leighton process at different values of diffusivity; blue: the reference diffusivity $\eta_t$ as given by Eq. (4.3), green: $2\eta_t$ (scaled by a factor of 2 to fit in the range), red: $\eta_t/2$ (scaled by a factor of 1/3). . . . .	75
4.2	Variation of saturated polar field strength $B_p$ with the flow amplitude $v_0$ , from a simulation in which a single BMR is placed at $15^\circ$ latitude. Red and blue colors correspond to simulations with and without the magnetic pumping. The data for latter case are multiplied by a factor of 60 for better visibility. . . . .	76
4.3	Variation of the polar field strength $B_p$ with the flow amplitude $v_0$ for three different cases in which the BMR is (a) placed at $5^\circ$ (blue), $15^\circ$ (red), and $30^\circ$ (green) latitudes, (b) experienced with three distinct diffusivity values; blue: $\eta_t$ —the reference diffusivity as given by Eq. (4.3), red: $2\eta_t$ , green: $\eta_t/2$ . Here, a single BMR is placed at $15^\circ$ latitude. . . . .	78

4.4	Top: Representation of the toroidal field $B_T$ (blue curve) in comparison with the poloidal field $B_P$ (gray curve, scaled by a factor of 2000) in relation with the flow amplitude. Bottom: Same as the top but the toroidal field variation from a set of simulations in which the same initial magnetic field is taken from the output of the simulation $v_0 = 8 \text{ m s}^{-1}$ . . . . .	80
4.5	Variation of the (a) mean magnetic fields and (c) cycle period with the flow speed. The right panels are same as the left ones but from a low diffusivity case ( $\eta_t/2$ ). . . . .	81
4.6	Variation of the latitudinal component of the surface meridional flow $v_\theta(R_s, 45^\circ)$ (red dashed curve) and the <i>radial</i> average of the poleward flow $\bar{v}_\theta^{\text{pole}}$ at $45^\circ$ latitude (blue dotted curve, scaled by a factor of 8) with the rotation period of the stars. . . . .	83
4.7	Same as Fig. 4.5, but from the set of simulations in which the meridional flow is taken from Kitchatinov & Olemskoy (2012b) mean-field hydrodynamics model of sun-like stars having rotation periods varying from 1–30 days. The horizontal axis represents the rotation period of the corresponding mean-field model of stars. . . . .	84
4.8	Time-latitude distribution of the surface radial magnetic field $B_r$ [in G] for stars of (a) 1 day, (b) 7 days, and (c) 25.38 days (solar value) rotation periods. . . . .	85
5.1	(a) Time-latitude distribution of the surface radial magnetic field $B_r$ [in kG], and (b) toroidal field along with starspot distribution (black dots) for a star of 1 day rotation period for Case I. . . . .	98
5.2	Same as Fig. 5.1, but for Case II. . . . .	98
5.3	Same as Fig. 5.1, but for Case III. . . . .	99
5.4	The variation of the mean peak field for a rotation period of 1 day with the $\zeta$ , the factor that shows the dependency of the rotation period on the tilt angle. . . . .	100

5.5	Time-latitude distribution of the surface radial magnetic field $B_r$ [in kG] for a star of 10 days rotation period for Cases I–III. . . . .	100
5.6	Time-latitude distribution of the surface radial magnetic field $B_r$ [in kG] for a star of 30 days rotation period for Cases I & III (Note: For stars with rotation periods $\geq 15$ days, Case III becomes identical to Case II). . . . .	102
5.7	Variation of the mean peak (a) toroidal and (b) poloidal magnetic fields with the rotation period of the star for different cases of simulations. The shaded area represents the range of rotation periods for which the spots are deposited in parallel to the rotation axis, i.e., void of low-latitude eruptions. . . . .	103
5.8	The variation of magnetic cycle period with the rotation period. . . . .	104
6.1	Time–latitude plots of toroidal field at $r = 0.71R_s$ (in the unit of $B_0$ ) for different stars with rotation period of (a) 1 day, (b) 7 days, (c) the solar value ( i.e., 25.38 days), and (d) 30 days for Model I. . . . .	117
6.2	Same as Fig. 6.1, but for Model II . . . . .	118
6.3	Same as Fig. 6.1, but from Model III. . . . .	118
6.4	Variations of the activity cycle period ( $P_{cyc}$ in years) with rotation period ( $P_{rot}$ in days) for (a) Models I (filled circles) and II (asterisks) and (b) Model III (solid and dashed lines are for northern and southern hemispheres, respectively). . . . .	120
6.5	Time series plot along with its smoothed variation of toroidal magnetic field for Model I of stars having rotation period of (a) 1 day, (b) 7 days, (c) 25.38 days (the solar value), and (d) 30 days. The dark-red bars highlight the extended weaker activity episodes i.e., grand minima in each case. . . . .	121
6.6	Same as Fig. 6.5 but computed from the absolute radial magnetic field, averaged over the whole surface for Model III. . . . .	122
6.7	Variation of Hurst exponent with respect to the rotation rate along with the linear-fit curve of all the models. . . . .	122

6.8 Change of (a) the number and (b) the average duration of grand minima with the rotation period of stars. Yellow circles, blue asterisks, and red diamonds depict the trends for Models I, II, and III, respectively. In (b), the error bars are computed from the standard deviation of the durations of the grand minima in each case. . . . . 122

6.9 Relation between frequency of occurrence of grand minima with the corresponding duration in Model I-III for the stars in which grand minima are observed. . . . . 126

7.1 Pictorial representation of the Babcock–Leighton dynamo model with anti-solar DR. (a) Initial poloidal field line. (b) and (c) This field is stretched by the anti-solar DR (equator rotates slower than poles) to produce a toroidal field. (d) The toroidal field rises to the surface and form tilted BMRs with loop structures. (e) Opposite polarity of sunspots connects near the equator and create a big poloidal loop (dashed line). (f) The large-scale poloidal field developed (dashed line) is in the same orientation as that of the original one. . . . . 132

7.2 Left: Radial variations of  $\alpha_{rr}$  (Eq. (7.4)) and  $\alpha_{\phi\phi}$  (Eq. (7.5)) at  $45^\circ$  latitude for  $\alpha_0 = 1 \text{ m s}^{-1}$ . Right: Latitudinal variations of the same at  $r = 0.95R_s$ . 134

7.3 Angular frequency  $\Omega/2\pi$  for the anti-solar DR; see Eq. (7.7). . . . . 135

7.4 Result of  $\alpha^2$  dynamo model with meridional circulation. Time-latitude diagrams of (a) toroidal magnetic field  $B$  at  $r = 0.7R_s$  and surface radial field  $B_r$ . All fields are measured with respect to  $B_0$ . . . . . 137

7.5 Butterfly diagram of the toroidal field averaged over a thickness of  $0.04R_s$  centered at  $0.71R_s$  (left) and  $0.85R_s$  (right) from stars of rotation periods 5, 10, 25.38 (Sun), 32, and 50 days (top to bottom); Runs A5, A10, A25, A32, and A50 . . . . . 140

7.6 Top–bottom: Dependences of the magnetic field, the ratio of toroidal to poloidal fields, and cycle periods with rotation periods of the stars. Circular and asterisk points are obtained from simulations in which DR decreases with rotation period through Eq. (7.8) (Runs A1–A50) and DR does not change (Runs B1–B50), respectively. Triangular points come from the same simulations as that of circular points but the meridional circulation is increased with rotation period through Eq. (7.10) (Runs C1–C50). The shaded area represents the solar-like DR regime, while the white space is anti-solar. . . . . 141

7.7 Simulation result of a star with rotation period 30 days in which the DR is made anti-solar during 10–14 years (identified by two vertical lines). Butterfly diagram of (a) the toroidal field at  $0.85R_s$  and (b) the same but averaged over a thickness of  $0.04R_s$  centered at  $0.71R_s$ . . . . . 144

7.8 Results from Run A32 computed over the whole CZ in the northern hemisphere: Temporal variations of (a) the toroidal field, (b) the mean effective latitudinal shear  $\frac{1}{r} \frac{\partial \Omega}{\partial \theta} / (1 + (B/B_0)^2)$  (in unit of  $10^{-9}$  nHz deg $^{-1}$ ), (c) the mean source term due to  $\alpha$  effect for the toroidal field ( $S_\alpha^{\text{Tor}}$  in Eq. (7.2) in unit of  $10^{-6}$ s $^{-1}$ ), and (d) the same as (a), but obtained from simulations in which there is no quenching in the shear (red dashed line) and  $\alpha_0 = 20$  m s $^{-1}$  (solid blue), instead of 80 m s $^{-1}$  which is used in all Runs A1–A50. . . . . 146

A.1 Time-latitude plot of the radial field from the 2D model with Babcock–Leighton  $\alpha$  for (a)  $v_0 = 4$  m s $^{-1}$  and (b)  $v_0 = 28$  m s $^{-1}$ . . . . . 171

A.2 Time-latitude plot of the radial field from the 3D STABLE model with a single BMR for (a)  $v_0 = 4$  m s $^{-1}$ , (b)  $v_0 = 8$  m s $^{-1}$ , and (c)  $v_0 = 28$  m s $^{-1}$ . 171

B.1 Left: Radial variations of  $\alpha_{rr}$  and  $\alpha_{\theta\theta}$  in m s $^{-1}$  at 45° latitude. Right: Latitudinal variations of the same at  $r = 0.95R_s$ . These are the profiles used in Set D; Eq. (7.12) with  $\alpha_0 = 1$  m s $^{-1}$ . . . . . 173

B.2 Variation of differential rotation ( $\Delta\Omega$ ) vs rotation period. The shaded area indicates the transition region to anti-solar differential rotation. . . . . 173

B.3 Solid line: diffusivity profile  $\eta$  used in all the sets of simulations, except Set E for which the profile shown by the dashed line is used. . . . . 174

B.4 Same as Fig. 7.5, but obtained from Runs E5, E17, E25, E32, E50 (top to bottom). . . . . 174

# List of Tables

- 3.1 Summary of all of the runs starting with weak seed field are listed along with the control parameters  $R_e, R_m, u_{\text{rms}}, \sigma$ . The table also contains the run time ( $T_r$  (in diffusion time scale), normalized temporal mean of the large-scale field  $\tilde{B}_{\text{rms}}$  and small-scale field,  $\tilde{b}$ , and their ratio. For Runs A–I,  $k_f = 3.1$  and  $\nu = 5 \times 10^{-3}$ , while in Run F',  $k_f = 5.1$  and  $\nu = 10^{-2}$ . For all the runs,  $P_m = 5$ . S/D denotes a stable or decaying solution. . . . 61
- 6.1 Summary of simulations. Here,  $P_{\text{rot}}$  is the rotation period of the star in days, and  $P_{\text{cyc}}$  is the mean magnetic cycle period in each hemisphere. For each model, the number of grand minima and parity are computed from the surface radial and the toroidal fields at the base of CZ, which are separated by a comma. . . . . 120
- 7.1 Summary of simulations. Here,  $T$  is the rotation period of star in days,  $P_{\text{cyc}}$  is the mean magnetic cycle period, SL and AS stand for solar and anti-solar DR, respectively. . . . . 139